JET–P(98)43

C F Maggi et al

The Isotope Effect on the L-mode Density Limit in JET H, D and T Divertor Plasmas

JET–P(98)43

The Isotope Effect on the L-mode Density Limit in JET H, D and T Divertor Plasmas

C F Maggi, R D Monk, L D Horton, K Borrass[1], G Corrigan, L C Ingesson, R König[1], G Saibene, R Smith, M Stamp, A Taroni, M von Hellermann.

JET Joint Undertaking, Abingdon, Oxfordshire, OX14 3EA,
[1]Max-Planck Institut für Plasmaphysik, Garching, Germany.

Preprint of a Paper submitted for publication in Nuclear Fusion

December 1998

ABSTRACT.

The first systematic study on the mass dependence of the L-mode density limit is reported for JET H, D and T divertor plasmas. The density limit, defined as the density at the onset of the X-point MARFE, is found to scale inversely with the ion mass in vertical target configurations, while no isotope effect is found in horizontal target configurations. 2D numerical simulations reproduce the observed mass dependence in vertical target discharges. The experiments indicate a coupling between the mass and power dependence of the L-mode density limit. The experimental results are compared with analytic models, which suggest that the ion-neutral transverse collisionality plays a role in the density limit.

1. INTRODUCTION

The maximum plasma density achievable in Ohmic/L-mode divertor discharges is determined by the formation of a MARFE in the X-point region [1-2], ultimately leading to a disruption. Prior to MARFE formation, the divertor plasma undergoes an increasing state of detachment characterized by substantial drops in both particle and energy fluxes to the target plates as well as in pressure along the magnetic field lines. Experimental studies of L-mode density limit discharges have been reported by various authors [2-5] and various scalings for the density limit have been proposed to explain the experimental findings [6-7].

While these studies mainly aimed at the scaling with discharge parameters such as heating power, safety factor (q_ψ) and toroidal field (B_t), recent experiments performed at JET with varying DT plasma fuelling mixtures [8-9], followed by a short campaign in hydrogen, have allowed for the first time a systematic investigation of the isotope scaling of density limits. This paper investigates the mass dependence of the L-mode density limit. Experiments devoted to the study of the isotope scaling of the H-mode density limit will be reported elsewhere.

2. EXPERIMENTAL RESULTS

2.1 Experimental Identification of the Density Limit

The time evolution of a typical JET L-mode density limit discharge with the MarkIIA divertor is shown in Fig. 1. As the plasma density is increased by gas fuelling at constant input power (in the case of the discharge of Fig. 1 Ohmic plus additional heating using neutral beams) the integral ion flux to the outer target plate, measured by Langmuir probes, initially increases, while that to the inner target remains low, indicating that the inner divertor leg is partially detached from the start. If the density is increased further, detachment is subsequently achieved at the outer divertor leg, by which time both particle and energy fluxes to the target have dropped dramatically. Throughout this time the total radiated power is always increasing.

In order to quantify the concept of divertor detachment we refer to the degree of detachment (DOD), as defined in [2]. It is the inverse ratio of the ion flux to the target measured by Langmuir probes to that expected in a high recycling regime, where it scales as the square of the plasma density according to a 2-Point model. The DOD is normalized at low density, where it is defined to be 1 (attached regime). For the example of Fig. 1 the DODs are given in the bottom panel.

When detachment is approached, the radiated power peaks, which in the early phase of the discharge are localized at the strike zones, converge towards the X-point region until a MARFE is formed, just above the X-point. This evolution is illustrated in Fig. 2 by tomographic reconstructions of the radiated power in the divertor measured by the bolometers. In contrast to MarkI Ohmic/L-mode density limit discharges, where the onset of the MARFE was a continuous and gradual process, in MarkIIA the

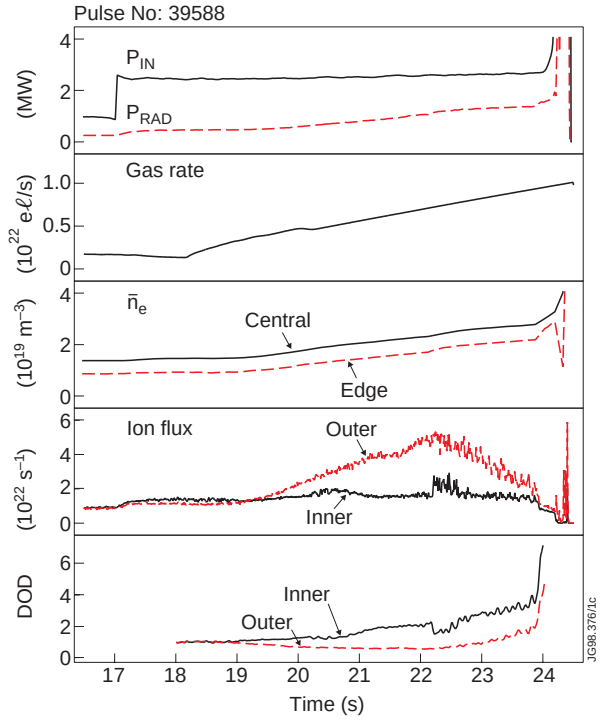

Figure 1. Time evolution of a typical L-mode density limit discharge in JET with the MarkIIA divertor (horizontal target configuration). From top to bottom: input and radiated power; gas fuelling rate; central and edge line averaged density; integrated ion flux to inner and outer divertor target; inner and outer target integral DOD.

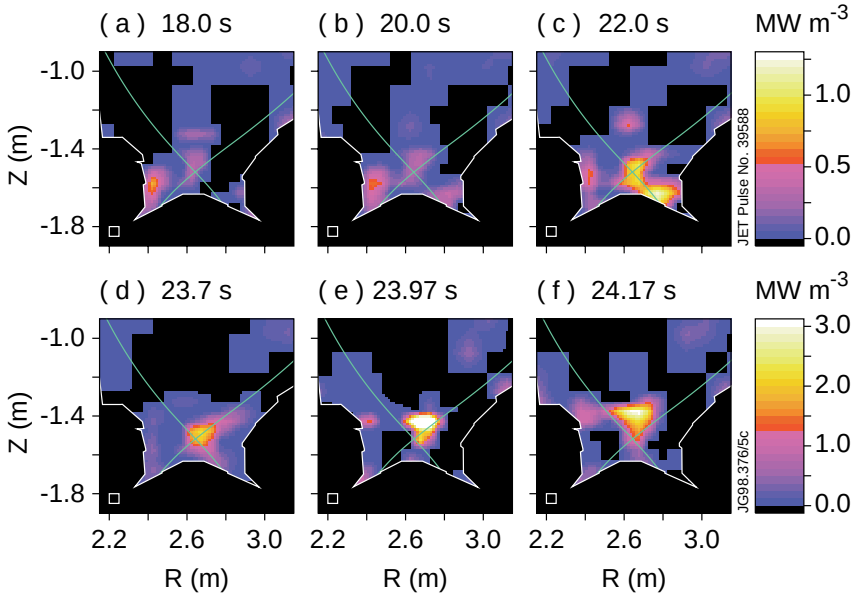

Figure 2. Tomographic reconstructions of total radiated power measured by the bolometers for the discharge of Fig. 1. The radiation peaks move from close to the target (a-b) up to the X-point (c-d). Subsequently, as the density is further increased, a MARFE is formed in the main plasma above the X-point (e-f). The square in the bottom left corner of each box represents the grid size of the tomographic reconstruction.

MARFE formation is a very sudden event. The time of the onset of the MARFE is marked by the first vertical line in Fig. 3, where we have expanded the time scale in the final phase of the discharge of Fig. 1. The onset of the MARFE coincides with complete detachment at the inner divertor leg (integral DOD ≅4-5). As the density is increased even further, the MARFE moves to the inner wall, eventually leading to a plasma disruption. By the time of the disruption the outer divertor leg is also completely detached.

This discussion suggests two possible choices for the density limit:

(i) the density at the point of the onset of the MARFE, which coincides with complete inner divertor detachment (in what follows called 'MARFE limit' or simply 'density limit')

(ii) the density that is reached when the disruption occurs (in what follows called the 'maximum density').

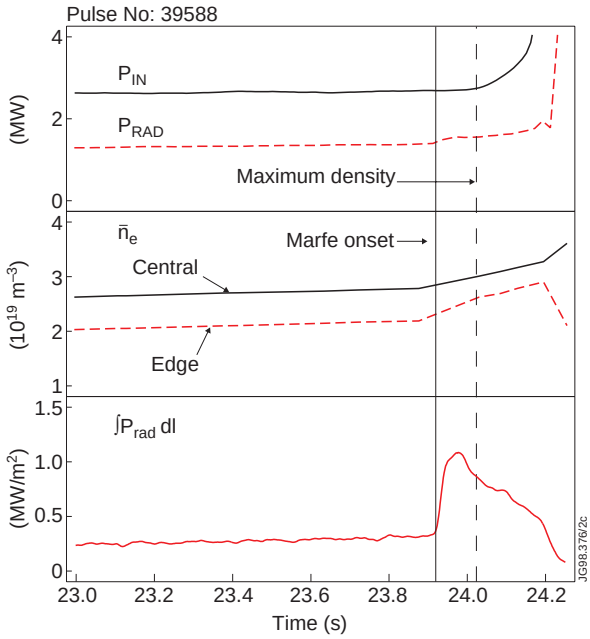

Figure 3. Expanded view of the final phase of the discharge of Fig.1, showing the experimental identification of the density limit, according to the onset of the MARFE (marked by the solid vertical line) or the maximum density obtained before the plasma disruption (vertical dashed line). The bottom panel shows the radiation flux measured by an in-vessel bolometer viewing the plasma horizontally just above the X-point.

These two density limits do not necessarily scale in a similar fashion, since they are driven by different physical mechanisms. In fact, while the 'MARFE limit' is governed by SOL physics, the 'maximum density' limit is also influenced by MARFE and/or core plasma physics. The importance of density limit lies in their character as operational limits. The window between MARFE formation and disruption may be rather narrow, particularly at low q_ψ, and stable operation in this window has not yet been proven. For the rest of the paper we therefore adopt (i) as the most adequate definition of density limit. Complete detachment defines a limit of the upstream separatrix density. A number of empirical studies have demonstrated that density limits are actually limits of the edge density and this further supports definition (i). A convenient byproduct of this choice is that fairly developed analytical gas target models exist and that this regime is well treated by 2D edge codes. This allows us to complement the experimental findings by detailed comparison with models.

Several measurements can be used to identify the 'MARFE limit' in a given discharge. The most straightforward to use is the radiated power flux measured by in-vessel divertor bolometers along lines of sight (LOS) which view the plasma horizontally above the X-point. The onset of the MARFE is clearly seen as a sudden jump in the radiation flux measured just

above the X-point (see bottom panel of Fig. 3). Correlated with this is the time evolution of the C II (λ = 6585 Å) and visible bremsstrahlung (λ = 5235 Å) photon flux profiles (not shown here), measured routinely by a CCD camera viewing poloidally across the whole divertor target from the top of the tokamak. The onset of the MARFE coincides with a sudden movement in the peak of the C II and bremsstrahlung photon fluxes from the outer target to the X-point. We define instead the 'maximum density' as the maximum value of the density just before the input power begins to rise strongly at the onset of the thermal collapse of the plasma. This is marked by the dashed vertical line in Fig. 3.

Since the density limit is a limit on the upstream separatrix density [10], ideally we would like to use this parameter in our study. However, the upstream separatrix density is not routinely measured in JET and therefore we use the line averaged density measured along the outermost channel of the far-infrared interferometer (see Fig. 4). We will refer to this measurement as the edge line averaged density (to distinguish it from the central line averaged density, which is measured along a chord through the centre of the core plasma). Also, reciprocating probe measurements in JET have shown that the separatrix density is proportional to the line averaged density in L-mode density limit discharges.

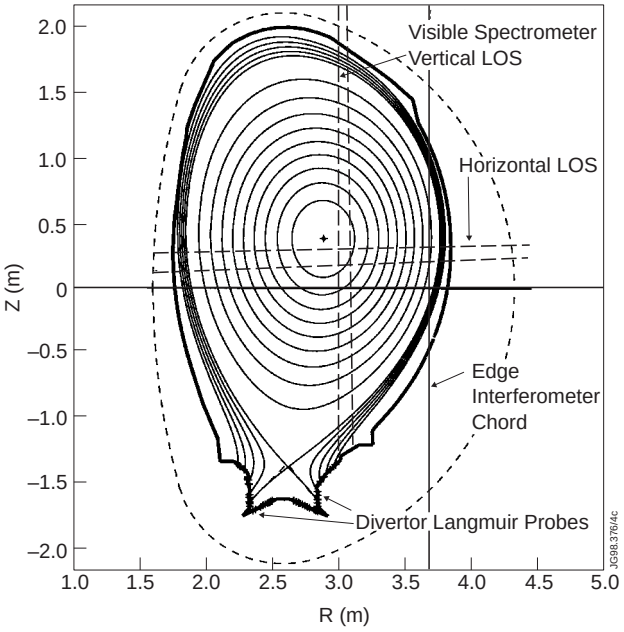

Figure 4. Poloidal cross section of the equilibrium reconstruction of a JET discharge showing the interferometer chord measuring the edge line averaged density, and the vertical and horizontal lines of sight of the visible spectrometer used for the measurements reported in section 2.4. Also shown is the array of fixed Langmuir probes embedded in the divertor target plates.

2.2 General Aspects of L-mode Density Limits in JET

Discharge parameters that may influence the density limit include, in particular, the net heating power, P_{net}, ($P_{net} = P_{in} - P_{rad}$, where P_{in} is the total input power and P_{rad} the total radiated power), the safety factor, q_ψ, and the toroidal field, B_t. In the database to be analysed q_ψ and B_t are essentially constant. Further impact, in addition to the ion mass, may arise through the divertor geometry. In JET two distinct divertors, the relatively open MarkI and the relatively closed MarkIIA were investigated [11]. Both permitted operation on vertical (V) and horizontal (H) plates. The flux expansion of the magnetic field in the divertor can be varied using the in-vessel divertor coils. In this paper horizontal configurations with two different flux expansions are considered. In the horizontal standard flux expansion equilibrium (H/SFE) the 2 cm SOL

surface, as measured from the separatrix at the outer midplane, is tangent to the vertical target plates of the divertor. In the low flux expansion equilibrium (H/LFE) the 2.5 cm SOL surface is tangent to the outer vertical target plate and the 3 cm SOL surface is still clear from the inner vertical target plate. The density limit observations made in the various configurations can be summarized as follows: the density limit has decreased by about a factor of 2 when going from the more open MarkI to the more closed MarkIIA divertor [11]. For a given divertor geometry the density limit is higher in vertical than in horizontal target SFE configurations. For horizontal target configurations, the density limit is higher in discharges with low divertor flux expansion. This is illustrated in Fig. 5, which shows the L-mode density limit database for MarkIIA (for all isotope masses) sorted by discharge configuration. These comprise vertical target, standard flux expansion (V/SFE), horizontal target standard (H/SFE) and low flux expansion (H/LFE). Fig. 5 also illustrates the power dependence of the density limit. The apparent scatter in the data, as will be explained in the following section, is due to the different isotope mass of the working gas used in the discharges. It is interesting to replot this set of discharges in the same edge density - P_{net} space, but at the 'maximum density' (Fig. 6) rather than at the 'MARFE limit'. The dependence of the density limit on divertor configuration has vanished (while the power dependence is still very clear), which suggests that MARFE and/or core plasma physics is at this stage determining the maximum achievable density, independently of the divertor geometry.

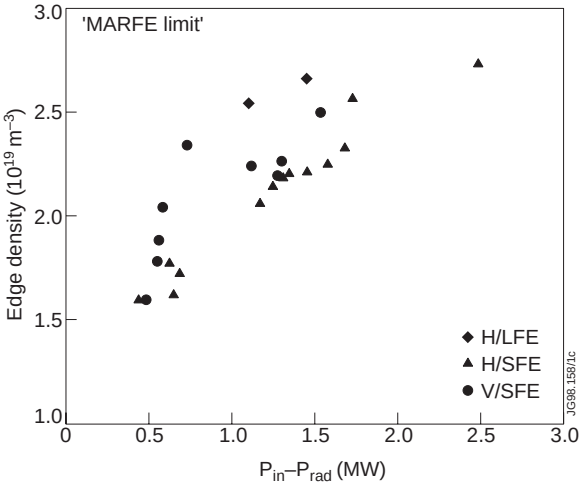

Figure 5. Edge line averaged density at the 'MARFE limit' versus net input power, $P_{net} = P_{in} - P_{rad}$, for the L-mode density limit discharges carried out in JET with the MarkIIA divertor (all isotope masses). The discharges are sorted by configuration: diamonds = horizontal target, low divertor flux expansion (H/LFE), triangles = horizontal target, standard flux expansion (H/SFE), circles = vertical target, standard flux expansion (V/SFE).

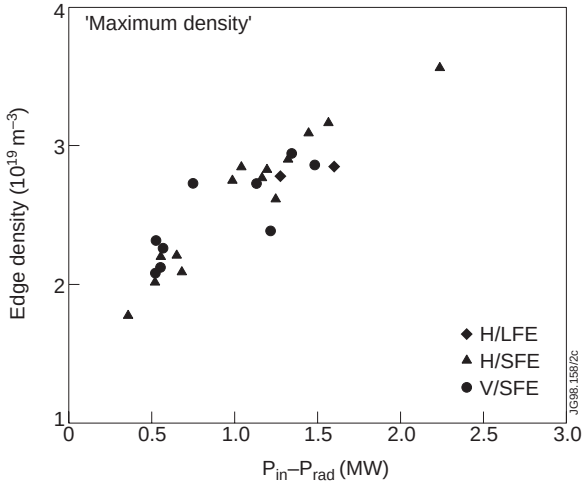

Figure 6. Edge line averaged density at the 'maximum density' limit plotted versus net input power, for the same set of discharges of Fig. 5. The discharges are sorted by configuration (symbols as in Fig. 5).

In this paper the isotope effect on the L-mode density limit in MarkIIA is investigated. This has been possible in JET as part of the recent DT experiments, which were followed by a short campaign with hydrogen plasmas. Therefore, with the same divertor geometry we have been able to measure the density limit of H, D, and T disruptive L-mode discharges. Based on recycling measurements in the divertor and at the plasma edge the T discharge was characterized by an isotope ratio of T/(H+D+T) = 0.9. For H and D plasmas this ratio was H or D/(H+D+T) $\geq$0.95.

2.3 Isotopic Effect on Plasma Detachment and Density Limit

Since the divertor configuration influences the density limit, as shown in the previous section, we have to study the mass dependence of the density limit separately for each configuration. The density limit database of Fig. 5 is thus plotted in Fig. 7 (a) and (b) for V/SFE and H/SFE configuration respectively, with the data sorted by isotope mass. All the discharges were carried out at a plasma current I_p= 2MA, toroidal field B_T= 2.5 T and $q_{95} = 4.0 \pm 0.3$. There is no distinction between Ohmic and additionally heated discharges in the onset of detachment and approach to the density limit, apart from the power dependence. Neutral beam heating was used for all discharges with additional heating, except one with ion cyclotron resonance heating, which nevertheless is, in all respects, similar to the other discharges.

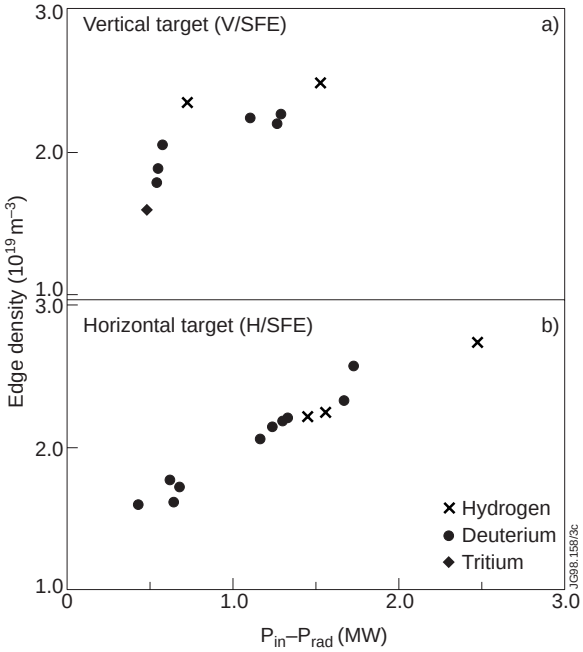

Figure 7. Edge line averaged density versus net input power at the 'MARFE limit' for (a) V/SFE and (b) H/SFE JET MarkIIA L-mode density limit discharges. The data are sorted by isotope mass: hydrogen (crosses), deuterium (circles) and tritium (diamonds).

It can be seen that whereas a clear isotope effect is found for V/SFE discharges, with the density limit increasing with decreasing hydrogenic mass at fixed net input power, the density limit in H/SFE discharges appears to be independent of the isotope mass. Note that the highest values of *Pnet* could only be accessed in hydrogen plasmas, due to the higher H-mode threshold at this plasma current and toroidal field [12]. In contrast, at 2MA/2.5T density limit discharges in tritium could only be obtained with Ohmic input power, due to the lower H-mode threshold found in tritium plasmas [13]. The injection of the power from one neutral beam source into such discharges (~1 MW) would trigger a transition into H-mode.

2.3.1 Vertical Target Discharges

The mass dependence of the density limit in vertical target L-mode discharges is a direct consequence of the mass dependence of divertor plasma detachment for a given upstream separatrix density. This is illustrated in Fig. 8 for three similar Ohmic discharges, with H, D and T plasmas respectively, where the inner target integral DOD is plotted versus central line averaged density. A similar behaviour is observed at the outer divertor (not shown). The integral ion flux to the innner and outer divertor targets for these discharges is shown in Fig. 9. Note the typical asymmetry and different detachment behaviour of inner and outer divertor legs. Fig. 10 shows the electron temperature, T_e, measured at the outer divertor target separatrix by the Langmuir probes for the three discharges. Although the probe interpretation in high density, low temperature regimes is problematic and leads to an overestimate of the electron temperature [14], it is nonetheless clear that for the same line averaged density T_e is lowest in T and highest in H plasmas, consistent with an earlier onset of detachment in T.

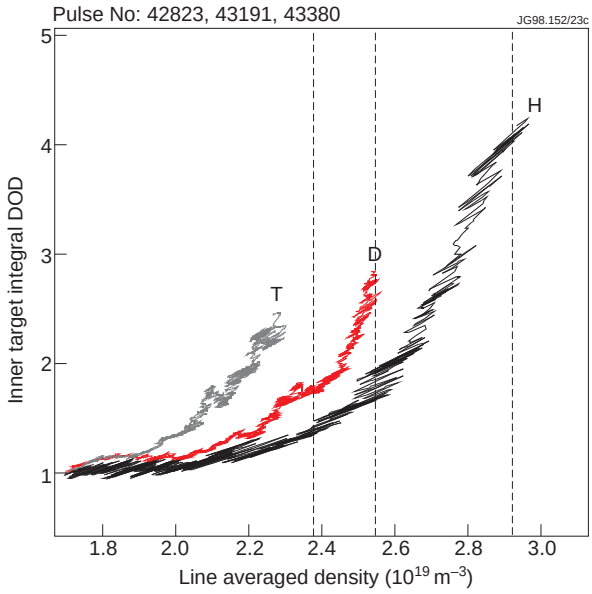

Figure 8. Inner target integral DOD versus central line averaged density for three similar Ohmic discharges in H, D, T (V/SFE configuration). The vertical dashed lines mark the results of the EDGE2D/NIMBUS simulations for the density limit in H, D, T (see section 3).

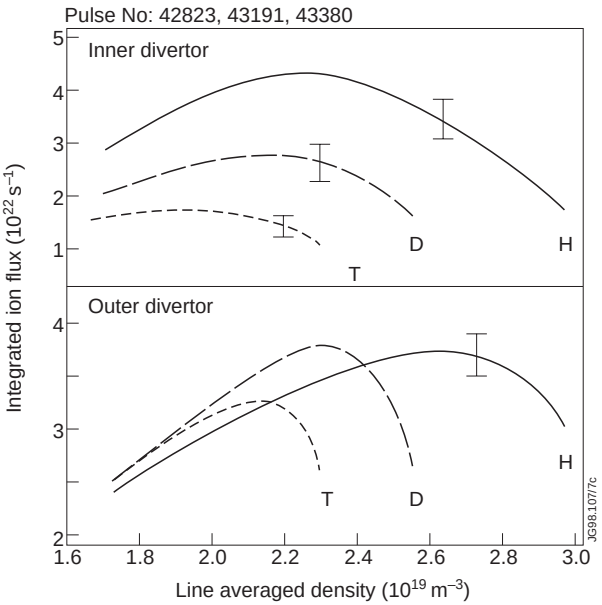

Figure 9. Integral ion flux to inner and outer divertor targets versus central line averaged density for the discharges of Fig. 8. The typical scatter of the data is shown by the error bars.

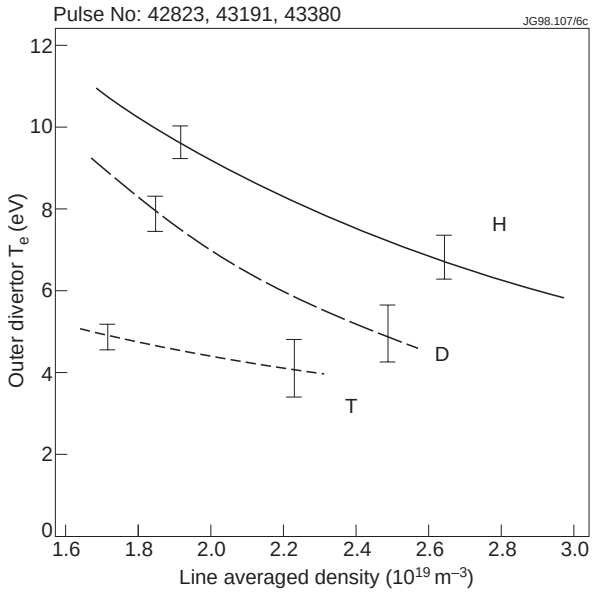

Figure 10. Outer target separatrix electron temperature, measured by the Langmuir probes, versus central line averaged density for the three discharges of Figure 8.

2.3.2 Horizontal Target Discharges

In contrast to what found for V/SFE discharges, in H/SFE discharges the density limit does not depend on the mass of the working gas. The reason for this is presumably the different detachment behaviour, with respect to isotope mass, observed for horizontal target configurations. This is illustrated in Fig. 11, which shows the inner and outer target integral ion flux for two similar L-mode density limit discharges in H and D. Whereas in V/SFE discharges detachment occurs in both divertor legs at progressively lower densities as the isotope mass of the plasma is increased, in H/SFE discharges this occurs in the outer divertor only, while the opposite effect is observed in the inner divertor. The inverse dependence of detachment on the hydrogenic mass in the two divertor legs is thought to explain the lack of mass dependence of the density limit in MarkIIA H/SFE discharges. However, the physical mechanism leading to such different detachment behaviour is not understood.

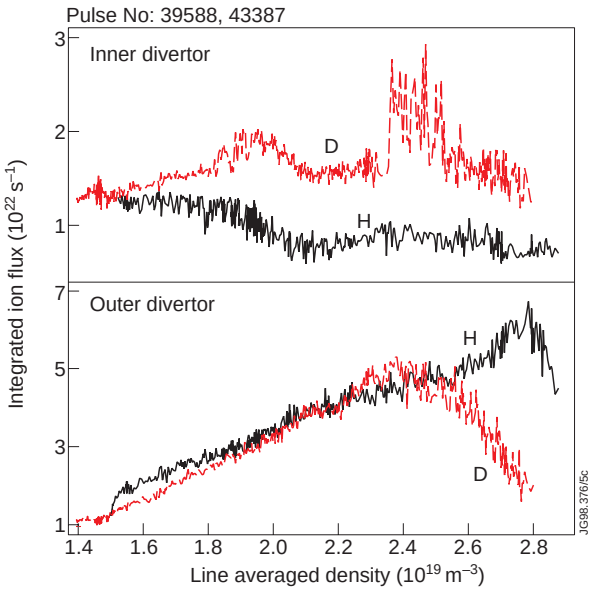

Figure 11. Inner and outer divertor integral ion flux versus central line averaged density for two similar discharges in H and D with H/SFE configuration showing an opposite dependence of detachment with isotope mass in the two divertor legs.

2.4 Impurity Behaviour

Carbon is the dominant intrinsic impurity in the density limit discharges studied in this paper. This is typical of all JET discharges without extrinsic impurity seeding [15]. The core carbon concentration, measured by visible charge exchange spectroscopy and by Z_{eff} (from visible bremsstrahlung emission), is systematically found to be lower in H than in D and T discharges. The core carbon concentration, C_C, measured by charge exchange at normalized minor radius $r/a = 0.26$, is essentially constant throughout the discharge. Despite the large error bars associated with the measurements at high density (the enhanced cooling of the edge results in additional complications in the interpretation of the charge exchange spectra), the carbon concentration is lower in H than in D discharges: typical values are $C_C(\%) = (0.2\pm0.1)$ for H and $C_C(\%) = (0.3\pm0.1)$ for D discharges at high density. Note that charge exchange measurements in T density limit plasmas could not be obtained due to the decreased H-mode threshold in T, which prevented the use of neutral beam additional heating in these discharges, as explained in section 2.3. The Z_{eff} measurements, plotted in Fig. 12 for V/SFE discharges, are consistent with the trend shown by the core carbon concentration (a similar behaviour is found for H/SFE discharges).

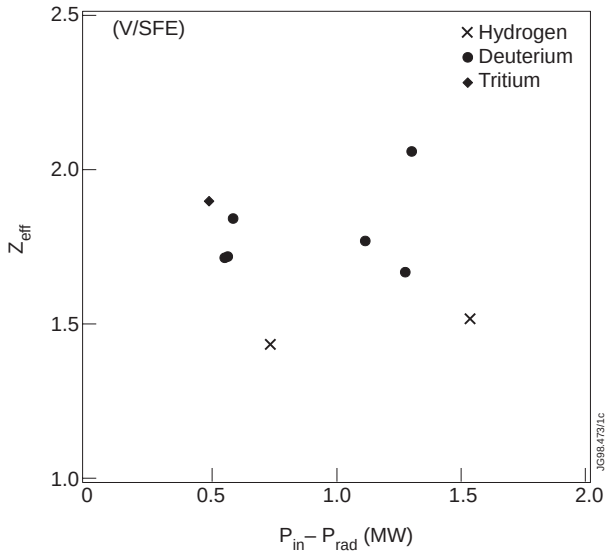

Figure 12. Z_{eff} measurements versus net input power at the density limit for V/SFE discharges: H (crosses), D (circles) and T (diamonds).

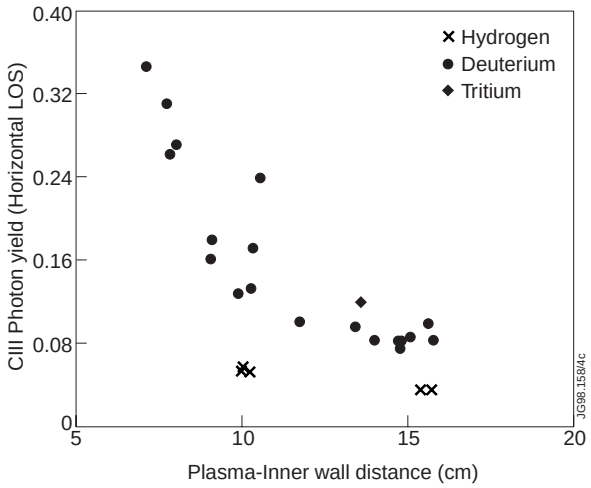

Figure 13. C III photon flux (λ = 4650 Å) normalized to Balmer-α photon flux, measured along the horizontal LOS shown in Fig. 4, versus plasma distance from the inner wall for H (crosses), D (circles) and T (diamonds) discharges (all configurations) at the density limit.

C III line emission at 4650 Å and Balmer-α emission is routinely measured using photomultiplier tubes coupled to interference filters along lines of sight (LOS) directed, amongst others, horizontally at the inner wall and vertically at the outer divertor shoulder, as illustrated in Fig. 4. The C III photon flux normalized to the Balmer-α photon flux measured along the vertical LOS is lowest in H and highest in T discharges, both in V/SFE and in H/SFE configurations. It is interesting to note that also the photon fluxes, which a priori are not a direct measure of carbon influxes from the vessel surfaces, decrease with decreasing plasma isotope mass in the same way as the core carbon concentration. The ratio of C III to Balmer-α photon flux measured along the horizontal LOS is found to depend primarily on the plasma distance from the inner wall (see Fig. 13). However, for plasma configurations that are well clear from the inner wall (i.e. for plasma-inner wall distances ≥10 cm) the C III normalized photon fluxes are consistently lower in H than in D and T plasmas.

A possible explanation for the observed trend of decreasing carbon concentration with decreasing plasma isotope mass could be the lower physical sputtering yield for carbon surfaces when bombarded by hydrogen rather than deuterium or tritium particle fluxes [16]. No mass dependence of the chemical sputtering yield for carbon is known to date. However, the relative importance of physically and chemically sputtered carbon sources from areas of the vessel that are and are not in direct contact with the plasma, and the link with their screening from the confined plasma are questions still far from being understood. Whereas this investigation goes beyond the scope of this paper, we need to address the role played by the impurities with respect to the different density limit observed as the isotope mass of the plasma is changed. This aspect

of the analysis will be addressed explicitly in connection with the interpretation of the experimental results by comparison with 2D modelling, which is the subject of the following section.

3. 2D NUMERICAL SIMULATIONS

We have carried out simulations of H, D and T plasmas using the EDGE2D/NIMBUS codes [17] for the Ohmic V/SFE configuration discharges of Fig. 8. The approach to detachment and to the density limit is sought by performing a series of runs to steady state in which the upstream separatrix density is progressively increased, while keeping all other input parameters fixed. Constant perpendicular transport coefficients are used, with $D_\perp = 0.1\ m^2 s^{-1}$ (for all ions) and $\chi_{e\perp} = \chi_{i\perp} = 1.5\ m^2 s^{-1}$. The input power crossing the separatrix is 1.2 MW (allowing for some small variation with increasing density, which is typical of Ohmic discharges) and is equally split between ions and electrons. A first series of density scans was carried out without carbon impurities (the 'pure plasma' case) in order to isolate the isotope effect of the pure plasma alone on the density limit.

Fig. 14 shows the inner divertor integral DOD for the pure plasma simulations plotted versus upstream separatrix density. As can be seen, the isotope effect on detachment found in experiment is qualitatively reproduced, with the onset of detachment (defined at integral DOD = 2) occurring at progressively lower separatrix densities as the isotope mass is increased from H to T. The maximum upstream separatrix density obtained in the simulations is limited by the onset of a 'Marfe-ing' behaviour, with strong ionization above the X-point and cooling of the edge plasma, which eventually makes the solution unstable. This defines the density limit in the simulations. The density limit in the simulations also decreases with increasing isotope mass, as found in experiment. Similar results are obtained for the outer divertor leg.

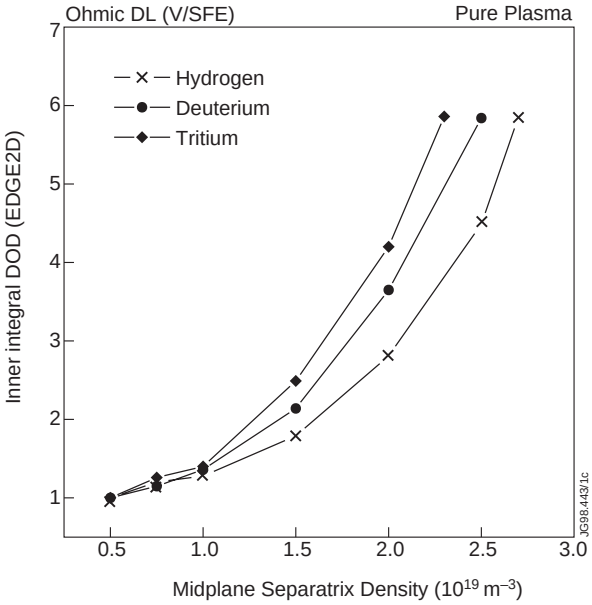

Figure 14. Inner divertor integral DOD from EDGE2D/NIMBUS simulations with pure plasma only versus upstream separatrix density for the discharges of Fig. 8.

As the mass of the hydrogenic species is increased the neutrals mean free path decreases, leading to larger neutral densities in the divertor with the heavier isotope. The higher neutral density and isotope mass in turn increase the ion-neutral charge exchange reaction rate, and thus more momentum is lost by the ions in T plasmas at a given upstream separatrix density. In other

words, the same momentum is lost in T at a lower separatrix density value than in D and H. This result could be a consequence of the increased divertor closure to neutrals with increasing plasma isotope mass for a given upstream density. Analogously, the increased recycling results in more energy loss from the plasma. Consequently, the onset of recombination, which is important at low divertor plasma temperature, occurs at a lower upstream density for the heavier isotope and the total particle recombination rate is highest for T and lowest for H plasmas.

In Fig. 15 we plot the fraction of hydrogen ionization above the X-point (hydrogen here denotes a generic hydrogenic isotope), which is our definition of divertor closure, versus upstream separatrix density for the pure plasma simulations. At low and medium upstream densities neutrals recycling at the divertor target plates escape more easily from the divertor region in the case of hydrogen plasmas. Conversely, in the same density range neutrals are retained best in tritium plasmas. At higher separatrix densities the divertor temperature decreases sufficiently so that the neutral mean free path increases and one reverts into an open divertor regime, with the neutrals escaping more freely into the main plasma and no distinction between plasmas with different isotope masses is found.

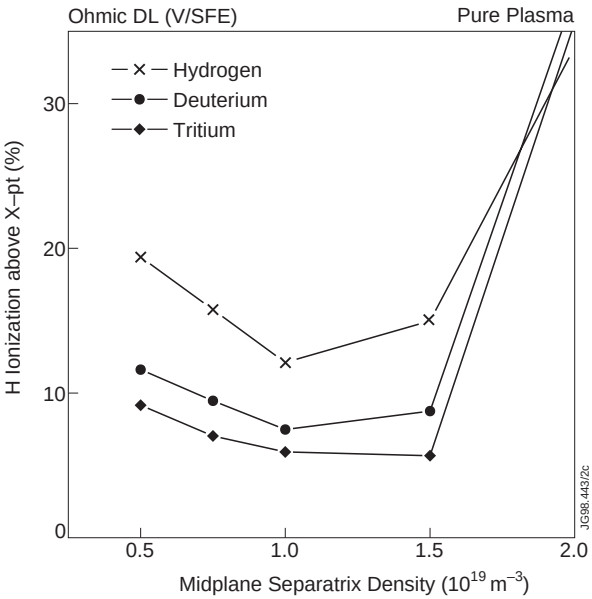

Figure 15. Fraction of hydrogen ionization above the X-point (i.e. divertor closure with respect to neutrals) versus upstream separatrix density from the EDGE2D/ NIMBUS pure plasma simulations.

The results discussed above do not depend on the choice of $M = 1$ (where M is the Mach number) as the boundary condition at the target plates in these simulations. In fact, tests were carried out to explicitly determine if part of the observed isotope effect was due to the mass dependence contained in the boundary condition. When a simulation is carried out with deuterium plasma, but imposing at the target the Mach number corresponding to tritium ions, the solution obtained is identical to that for a deuterium plasma with the proper boundary condition. The only difference is a small variation of the ion flow velocity in the vicinity of the target plates (i.e. in the first few cells of the grid close to the target), which vanishes further upstream.

Whereas analysis of the pure plasma simulations is useful in bringing out the role of the hydrogenic plasma in the mass dependence of the density limit, in the absence of impurity radiation it is not possible to carry out a realistic comparison between the simulations and the actual experiment. Therefore a second series of simulations was carried out with carbon impurities. In the simulations carbon production is obtained by physical sputtering (the sputtering yield data of [16] are used) plus a constant offset - $Y_{chem}^{eff} = 2\%$, to match the total radiation in the

experiment - which approximates the contribution of chemical sputtering. This is necessary to produce carbon sources at low temperature, when physical sputtering becomes negligible. The results of the EDGE2D/NIMBUS simulations for the density limit in H, D and T (vertical dashed lines) are overlayed on the experimental DOD in Fig. 8. These results have been normalized to the D simulation, since the ratio of separatrix to central line averaged density was not measured for these pulses. With this normalization, the separatrix density in the EDGE2D simulations is 60% of the central line averaged density. It can be seen that the 2D numerical simulations reproduce the trend found in experiment. Quantitative comparison with the experiment, however, shows that the 2D simulations fail to reproduce the details of the approach to detachment and the inner/outer divertor detachment asymmetry in V/SFE discharges. This is illustrated in Fig. 16, showing the simulated ion fluxes to the divertor targets, to be compared with the measurements plotted in Fig. 9. The detailed simulation of actual density limit discharges still presents difficulties and discrepancies with experiment [18]. However, progress in this area is being made. The 2D codes are robust with respect to relative trends and it is in this context that we compare the EDGE2D/NIMBUS simulations with experiment in this paper.

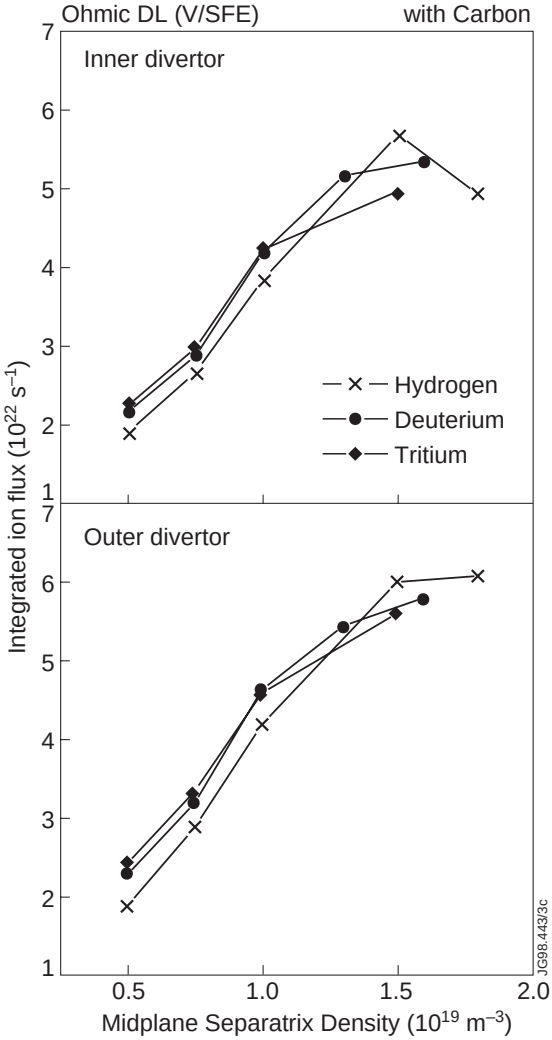

Figure 16. Integral ion fluxes to inner and outer divertor from EDGE2D/NIMBUS simulations in H, D and T.

Although the physical sputtering yield decreases with decreasing isotope mass at a given energy [16], in the simulations the isotope effect on detachment is obtained at high density, where physical sputtering is negligible and the carbon source is entirely dominated by chemical sputtering, for which no mass dependence has been assumed. The simulations also give a similar trend of impurity behaviour with respect to plasma ion mass as the experiment. For instance, the C III photon yield measured along the vertical LOS is consistently highest in T and lowest in H at any given density and this trend is also obtained in the simulations. This shows that at high density the C III photon yield is not a measurement of the carbon influx, since $Y_{eff} = 2\%$ is assumed for all three isotopes.

To conclude, the fact that both the pure plasma simulations and those with carbon impurities show an isotope effect of the density limit indicates that the impurities alone cannot be responsible for this effect. In addition, if the impurities alone were responsible for the different density limit in H, D and T V/SFE plasmas through the different radiated power, this would fall into the dependence of the density limit on P_{net} and there would be no explicit mass dependence in the experimental data, as instead shown in Fig. 7. Also, the trend of lower carbon concentration and photon fluxes in H than in D and T plasmas is observed both in V/SFE and H/SFE discharges, but an isotope effect on the density limit is measured only for V/SFE pulses.

Density scan simulations of H and D pure plasmas with H/SFE configuration do not reproduce the inverse dependence of detachment on the hydrogenic mass in the two divertor legs, which is observed experimentally in this configuration. The reason for this is not understood, but it may be related to details of neutral recycling in the inner divertor corner (which results from the inclination of the targets in the MarkIIA geometry) not reproduced in the codes.

4. COMPARISON WITH ANALYTICAL THEORY

In this section we compare our experimental results with the analytical model for the detachment limit proposed in Ref. [10], which can be extended in a straightforward manner to include isotope dependencies. Starting from the basic equations of a 2-Point model applied to the region upstream of the gas target, assuming Bohm-type perpendicular transport and showing that at complete detachment M^* and γ^* (the Mach number and the sheath transmission coefficient at the gas target entrance) are solely functions of the ion-neutral transverse collisionality at the gas target entrance, one obtains a relation for the upstream separatrix density at complete detachment, n_S^{det} (see Eq. (13) of [10]):

$$n_S^{det} \propto m^{11/32} \frac{B_t^{5/16} q_\perp^{5/8}}{L^{1/16}} \frac{T^{*11/32}}{\left\{ M^*(\nu_{n-i}^*) \left[\xi^* + T^* \gamma^*(\nu_{n-i}^*) \right] \right\}^{11/16}} \qquad (1)$$

Here superscript * denotes quantities at the gas target entrance, B_t is the toroidal magnetic field on axis, $q_\perp$ the power flux across the separatrix, T^* the temperature ($T^* \cong$ const ($\cong 5$ eV)), $L \cong \pi q_\psi R$ the connection length and ξ^* the mean energy consumed per ionization event ($\xi^* \cong 30$ eV). ν_{n-i}^* is the ion-neutral transverse collisionality,

$$\nu_{n-i}^* = \frac{\Delta_n^*}{\lambda_{n-i}^*} \propto \frac{q_\perp^{1/11} n_S^{det\ 16/11} L^{12/11}}{B_t^{5/11}} \qquad (2)$$

where Δ_n^* is the density decay length and λ_{n-i}^* the neutral mean free path with respect to ion-

neutral collisions (charge exchange and elastic) [10]. The explicit mass dependence is introduced in Eq. (1) through the ion sound speed at the gas target entrance. This is not in contradiction to what is discussed in section 3, where the mass dependence of the boundary condition at the target plates was tested in the numerical simulations. Instead there is no boundary condition on M^*, which is a strongly varying quantity. Additional mass dependencies are contained in ν^*_{n-i}. If Bohm-type perpendicular transport is assumed as an example, there is no mass dependence in Δ^*_n, whereas one has for the neutral mean free path:

$$\lambda^*_{n-i} = \frac{v^*_{th}}{n^* < \sigma v >^*_{n-i} (T^*, m)} \propto \frac{T^{*1/2}}{m^{1/2}\, n^* < \sigma v >^*_{n-i} (T^*, m)} \tag{3}$$

with v^*_{th} the neutral thermal speed and $< \sigma v >_{n-i} (T, m)$ the combined charge exchange and elastic rate coefficient. Following Ref. [19] one can make the 'ansatz'

$$< \sigma v >_{n-i} (T, m) \propto \left(\frac{T}{m} \right)^{\mu} \tag{4}$$

where $\mu = 0.2$ gives a reasonable fit. This results in (see Eq. (1)):

$$\nu^*_{n-i} \propto \frac{q_\perp^{1/11}\, n_S^{det\ 16/11}\, L^{12/11}}{B_t^{5/11}}\, m^{1/2-\mu} \tag{5}$$

and

$$n_S^{det} \propto m^{11/32}\, \frac{B_t^{5/16} q_\perp^{5/8}}{L^{1/16}}\, T^{*11/32} \times$$
$$\left\{ M^* \left(q_\perp^{1/11} n_S^{det\ 16/11} L^{12/11} B_t^{-5/11} m^{1/2-\mu} \right) \left[\xi^* + T^* \gamma^* \left(q_\perp^{1/11} n_S^{det\ 16/11} L^{12/11} B_t^{-5/11} m^{1/2-\mu} \right) \right] \right\}^{-11/16} \tag{6}$$

The model cannot provide an explicit expression for n_S^{det} because of the lack of information on the type of dependence of M^* and γ^* on the ion-neutral transverse collisionality. Proceeding by analogy with Ref. [10], i.e. assuming that the density limit of Eq. (6) is of the power law type (in analogy with Eq. (14) of [10]), one obtains

$$\frac{T^{*11/32}}{\left\{M^{*}(\nu^{*}_{n-i})\left[\xi^{*}+\gamma^{*}(\nu^{*}_{n-i})T^{*}\right]\right\}^{11/16}} \propto \left(q_{\perp}^{1/11} n_S^{det\ 16/11} L^{12/11} B_t^{-5/11} m^{1/2-\mu}\right)^{-\beta\, 11/16} \quad (7)$$

where β is an undetermined constant. This results in the following class of scalings for n_S^{det}:

$$n_S^{det} \propto \frac{q_{\perp}^{x}\, B_t^{5/16}}{(q_{\psi} R)^{11/16\ -x}}\ m^{0.8x-0.16} \quad (8)$$

where $x = \frac{10-\beta}{16(1+\beta)}$ and $\mu = 0.2$ was used. Since our density limit database with the MarkIIA divertor is at fixed toroidal field (B_t = 2.5 T) and at fixed q_{ψ} (q_{95} = 4.0 ±0.3), we are effectively interested in the comparison of the experimental data with a predicted scaling of the type:

$$n_s \propto q_{\perp}^{x} m^{0.8x-0.16}. \quad (9)$$

The relations obtained so far depend on the assumption made for perpendicular transport. If constant perpendicular transport ($D_{\perp} = const$, $\chi_{\perp} = const$) is adopted instead of Bohm, one obtains instead of Eq. (8):

$$n_S^{det} \propto q_{\perp}^{x}\ m^{0.8x-0.25} \quad (10)$$

where now $x = \frac{10+\beta}{14(1+\beta)}$. The main result of Eqs. (9) and (10) is the coupling between power and mass dependence of the density limit. We thus perform a linear regression of our experimental data to a power law function of the type $n_s \propto q_{\perp}^{x}\, m^{y}$, with separate fits for the different divertor configurations (V/SFE and H/SFE discharges), obtaining:

$$n_s = (1.79 \pm 0.22)\ q_{\perp}^{0.18\pm0.05} m^{-0.2\pm0.06} \qquad \text{for V/SFE} \quad (11)$$

$$n_s = (2.4 \pm 0.13)\ q_{\perp}^{0.34\pm0.03}\, m^{-0.02\pm0.05} \qquad \text{for H/SFE} \quad (12)$$

where we have assumed implicitly a direct proportionality between edge line averaged density and upstream separatrix density (which is not measured, as discussed in Section 2.1) and $q_{\perp} = (P_{in} - P_{rad})/A_{plas}$, with $A_{plas}\left[m^2\right]$ the area of the plasma. The results of the fits to the experimental data of Fig. 7 are shown in Fig. 17 (a) and (b). Eqs. (11) and (12) indicate a relation between power and mass dependence of the form suggested by Eqs. (9) and (10).

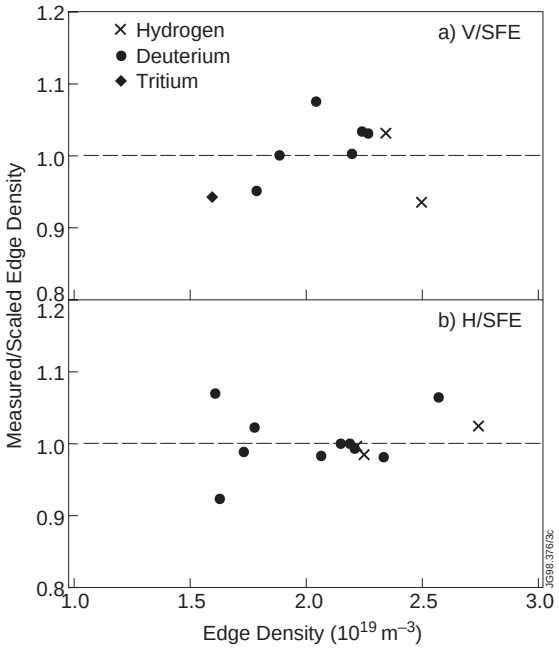

Figure 17. Ratio of measured edge density to scaled edge density, obtained from the fit of the experimental data to a power law of the type $n_s \propto q_\perp^x m^y$*, versus measured edge density for (a) V/SFE and (b) H/SFE discharges. The data are sorted by isotope mass: H (crosses), D (circles), T (diamonds).*

If we use in Eqs. (9) and (10) the values for x obtained from the fit to the experimental data, x=0.18 for V/SFE and x=0.34 for H/SFE discharges, the model with constant perpendicular transport provides rather good agreement with the measurements, while the scaling with Bohm transport gives less good agreement. Although this result should not be regarded as an argument to support one particular type of perpendicular transport, it is an interesting illustration of the effect introduced in the scalings by the uncertainties in the transport.

5. CONCLUSIONS

Operation with hydrogen, deuterium and tritium plasmas during the JET MarkIIA divertor campaign has provided an ideal scenario for the investigation of the isotope scaling of a variety of plasma regimes. In this paper we have reported a study of the mass dependence of disruptive L-mode density limits.

Experiments in V/SFE discharges have shown a clear isotope effect on plasma detachment and the density limit. The density limit decreases as the hydrogenic mass is increased. In contrast, no isotope effect is found in H/SFE discharges. This is presumably due to the fact that in this configuration the onset of detachment scales with isotope mass in the inner divertor leg and inversely with mass in the outer divertor. This effect is not understood and is not reproduced in the simulations.

EDGE2D/NIMBUS simulations of density scans in pure plasmas reproduce the trend in the observed isotope effect on the density limit in V/SFE discharges. Simulations with carbon impurities are in good agreement with experiment. The isotope effect on the density limit is not

much larger than found in the pure plasma simulations. There is some increase in the difference between H and D density limit when impurities are included in the simulations. This may be due to the impurity content and radiated power of H plasmas being somewhat lower than in similar D and T pulses, both in experiment and simulation.

The experimental data indicate a coupling between net input power and mass dependence of the density limit, as predicted by the analytical model. Fitting the experimental data to a power law function of the type $n_S \propto q_\perp^x m^y$, leads to a scaling for the upstream density at the density limit of $n_S \propto q_\perp^{0.18\pm0.05} m^{-0.2\pm0.06}$ for V/SFE discharges and of $n_S \propto q_\perp^{0.34\pm0.03} m^{-0.02\pm0.05}$ for H/SFE discharges. In the analytical model this coupling between power and mass dependence of the density limit originates from the ion-neutral transverse collisionality at the ionization front in the divertor. The experimental findings thus suggest that the ion-neutral transverse collisionality may play a role in determining the disruptive L-mode density limit.

REFERENCES

[1] LIPSCHULTZ, B. et al., Nucl. Fusion 24 (1984) 977.

[2] LOARTE, A., et al., Nucl. Fusion **38** (1998) 331.

[3] PETRIE, T.W., et al., Nucl. Fusion **33** (1993) 929.

[4] CAMPBELL, D.J., et al., in Controlled Fusion and Plasma Physics (proc. 21st Eur. Conf. Montpellier, 1994) Vol 18B, I-2.

[5] MERTENS, V., et al., Nucl. Fusion **37** (1997) 1607.

[6] AXON, K.B., et al., in Plasma Physics and Controlled Nuclear Fusion Research 1980 (proc. 8th Int. Conf. Brussels, 1980), Vol. 1, IAEA, Vienna (1981) 413.

[7] GREENWALD, M., et al., Nucl. Fusion **28** (1988) 2199.

[8] JACQUINOT, J., et al., 'Overview of ITER physics deuterium-tritium experiments in JET', submitted to Nucl. Fusion, 1998.

[9] KEILHACKER, M., and the JET TEAM, 'High fusion performance from deuterium-tritium plasmas in the JET tokamak', submitted to Nucl. Fusion, 1998.

[10] BORRASS, K., et al., Nucl. Fusion **37** (1997) 523.

[11] HORTON, L.D., et al., 'Studies in JET Divertors of varied geometry I: non seeded plasma operation', submitted to Nucl. Fusion, 1998.

[12] ASDEX TEAM, Nucl. Fusion **29** (1989) 1959.

[13] RIGHI, E., et al., 'Isotope scaling of the H-mode power threshold in tritium, deuterium-tritium, deuterium and hydrogen plasmas on JET', submitted to Nucl. Fusion, 1998.

[14] MONK, R.D., et al., Contrib. Plasma Phys. **36** (1996) 37.

[15] McCRACKEN, G.M., et al., 'Studies in JET Divertors of different geometry III: Intrinsic Impurity Behaviour', submitted to Nucl. Fusion, 1998.

[16] ECKSTEIN, W., et al., Sputtering Data, IPP-9/82, 1993.
[17] SIMONINI, R., et al., Contr. Pl. Physics **34**, No 2-3 (1984) 368.
[18] MAGGI, C.F., et al., submitted to J. Nucl. Mater. (1998), Proc. 13th PSI Conf., San Diego, 1998.
[19] BACHMANN, P., and BELITZ, J.H., 'Elastic Processes in Hydrogen-Helium Plasmas: Collision Data', Report IPP 8/2 (1993).